Available online at www.sciencedirect.com
SCIENCE DIRECT®
International Journal of Solids and Structures 42 (2005) 2965–2975
INTERNATIONAL JOURNAL OF SOLIDS and STRUCTURES
www.elsevier.com/locate/ijsolstr

Loading-carrying welds joints analysis using boundary element method

Xu Kai *, Lu Yong, S.T. Lie

School of Civil and Environmental Engineering, Nanyang Technological University, 50 Nanyang Avenue, Singapore 639798, Singapore

Received 12 December 2003; received in revised form 5 October 2004
Available online 18 November 2004

Abstract

The behavior of loading-carrying welds joints has been studied extensively using boundary element method. The symmetric boundary element method for multiple cracks problem is derived using Betti's reciprocal theorem. The analysis can be performed effectively in single domain. High order element is proposed to solve the double integrals. The stress intensity factors are calculated for weld root and weld toe and the critical value for class F2 and W are obtained. Formulation for the critical value is obtained for the engineering design. The results are compared with those obtained by dual boundary element method and derived from the code of practice. Finally, the theoretical fatigue life of such joints is estimated.

Keywords: Stress intensity factor; Magnification factor; Fatigue life; SGBEM

1. Introduction

In general, the load-carrying fillet welded joints is frequently found when the longitudinal stiffener is welded to a transverse stiffener in a girder web of steel bridges as shown in Fig. 1. The design of load-carrying fillet welded joints under fatigue loading conditions is very complicated. There are two stress concentrations from which fatigue cracks can initiate. These are the severe crack-like internal notch formed by the plate end at the root of the weld and the weld toe. Which of these two points is most likely to initiate failure depends greatly upon the relative magnitude of the nominal stress in the plate and nominal stress in the weld. These relative stresses influence the likely failure initiation points. The value of the stress at the root

* Corresponding author. Tel.: +65 6790 6913; fax: +65 6791 0676.
E-mail address: ckxu@ntu.edu.sg (X. Kai).

0020-7683/$ - see front matter © 2004 Elsevier Ltd. All rights reserved.
doi:10.1016/j.ijsolstr.2004.10.005

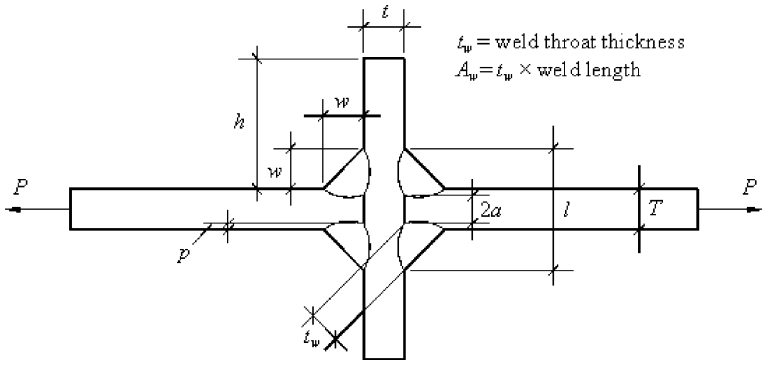

Fig. 1. Load-carrying fillet welds joint.

related to that at the toe depends on the ratio of $w = \lambda T$, and when the ratio λ is large, failure will always occur at the toe of the weld. When the ratio of λ is small, stress at the tip of the root defect may be high enough to propagate a crack from the defect so as to cause failure there before failure at the weld toe. When this happens, the fillet weld joint is classified as Class W (BS7608, 1993), Otherwise it still falls under Class F2 (BS7608, 1993).

Boundary element method had been found to be attractive for analyzing this type of welded joints (Lie and Bian, 1997). In this paper, symmetric boundary element method (SGBEM) is used to analyzing load-carrying weld joints containing multiple cracks. Direct SGBEM for multiple cracks problem is derived using the Betti's reciprocal theorem for domain containing any number of traction-free cracks. Auxiliary fictitious state is used to derive the main formulations, and it has been shown earlier by Lie et al. (1999) that this approach simplifies the derivation procedure considerably for a domain containing several traction-free cracks. High order element interpolation is proposed and yields good adaptability and reduces the computational cost. The load-carrying fillet welded joint containing several cracks has been analyzed, and the stress intensity factors (SIF) at the crack tips have been compared with the dual boundary element methods results. The results of a detailed numerical analysis of load-carrying fillet welded joints using symmetric Galerkin boundary element method are obtained to determine the critical value of $\gamma = 2a/T$ and $\lambda = w/T$ for a fixed value of $\beta = t/T$ so that the crack will propagate from the weld root. The stress intensity factors and the magnification factors M_k, obtained from the symmetric Galerkin boundary element method (SGBEM) are compared with that results obtained using dual boundary element method (Lie and Bian, 1997), and BS7608 (1993).

2. Boundary element method

Using an asterisk and non-asterisk notations as the auxiliary fictitious and actual state respectively in Fig. 2, the Betti's reciprocity identity at the fictitious state for domain containing three cracks can be written as:

$$\int_{\Gamma^*} \left([\mathbf{F}^*]^{\mathrm{T}} \mathbf{D} - [\mathbf{D}^*]^{\mathrm{T}} \mathbf{F} \right) \mathrm{d}\Gamma^*_{\xi} = \int_{\Gamma^*_{c1}} \left([\mathbf{F}^*]^{\mathrm{T}} \mathbf{U} - [\mathbf{U}^*]^{\mathrm{T}} \mathbf{F} \right) \mathrm{d}\Gamma^*_{c1} + \int_{\Gamma^*_{c2}} \left([\mathbf{F}^*]^{\mathrm{T}} \mathbf{V} - [\mathbf{V}^*]^{\mathrm{T}} \mathbf{F} \right) \mathrm{d}\Gamma^*_{c2} + \int_{\Gamma^*_{c3}} \left([\mathbf{F}^*]^{\mathrm{T}} \mathbf{W} - [\mathbf{W}^*]^{\mathrm{T}} \mathbf{F} \right) \mathrm{d}\Gamma^*_{c3} \quad (1)$$

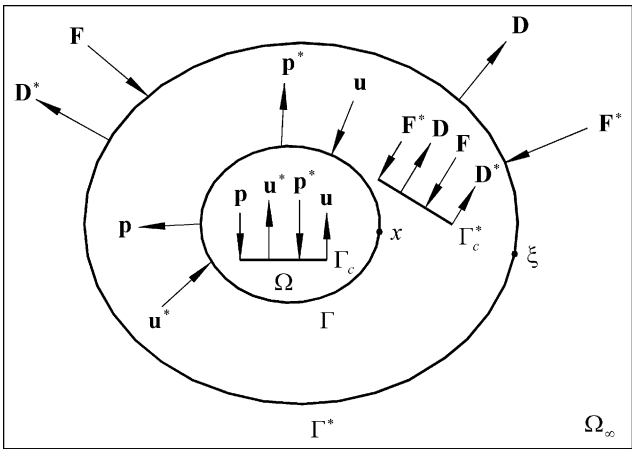

Fig. 2. Domain Ω containing a crack Γ_c embedded in Ω_∞ with the traction $\mathbf{F}^*$ and displacement $\mathbf{D}^*$ sources acting along the fictitious boundary Γ^*.

where $\mathbf{D}$ and $\mathbf{F}$ are displacements and traction vectors along the fictitious boundary Γ^*, and $\mathbf{U}$, $\mathbf{V}$ and $\mathbf{W}$ are the crack opening displacements along the fictitious crack surfaces Γ^*_{c1}, Γ^*_{c2} and Γ^*_{c3} respectively. The external actions consisting of displacement discontinuities $\mathbf{u}$ and forces $\mathbf{p}$ distributed along Γ. The displacements and tractions at the field point $\boldsymbol{\xi}$ due to the above external actions can be given by the following expressions:

$$\mathbf{D}(\boldsymbol{\xi}) = \int_{\Gamma_x} [\mathbf{G}_{uu}(\xi, \mathbf{x})\mathbf{p}(\mathbf{x}) - \mathbf{G}_{up}(\boldsymbol{\xi}, \mathbf{x}; \mathbf{v}, /)\mathbf{u}(\mathbf{x})]\, \mathrm{d}\Gamma_x + \int_{\Gamma_{c1}} \mathbf{G}_{up}(\boldsymbol{\xi}, \mathbf{x}; \mathbf{v}, /)\mathbf{U}(\mathbf{x})\, \mathrm{d}\Gamma_{c1} + \int_{\Gamma_{c2}} \mathbf{G}_{up}(\boldsymbol{\xi}, \mathbf{x}; \mathbf{v}, /)\mathbf{V}(\mathbf{x})\, \mathrm{d}\Gamma_{c2} + \int_{\Gamma_{c3}} \mathbf{G}_{up}(\boldsymbol{\xi}, \mathbf{x}; \mathbf{v}, /)\mathbf{W}(\mathbf{x})\, \mathrm{d}\Gamma_{c3} \tag{2}$$

$$\mathbf{F}(\boldsymbol{\xi}) = \int_{\Gamma_x} [\mathbf{G}_{pu}(\boldsymbol{\xi}, \mathbf{x}; /, \mathbf{n})\mathbf{p}(\mathbf{x}) - \mathbf{G}_{pp}(\boldsymbol{\xi}, \mathbf{x}; \mathbf{v}, \mathbf{n})\mathbf{u}(\mathbf{x})]\, \mathrm{d}\Gamma_x + \int_{\Gamma_{c1}} \mathbf{G}_{pp}(\boldsymbol{\xi}, \mathbf{x}; \mathbf{v}, \mathbf{n})\mathbf{U}(\mathbf{x})\, \mathrm{d}\Gamma_{c1} + \int_{\Gamma_{c2}} \mathbf{G}_{pp}(\boldsymbol{\xi}, \mathbf{x}; \mathbf{v}, \mathbf{n})\mathbf{V}(\mathbf{x})\, \mathrm{d}\Gamma_{c2} + \int_{\Gamma_{c3}} \mathbf{G}_{pp}(\boldsymbol{\xi}, \mathbf{x}; \mathbf{v}, \mathbf{n})\mathbf{W}(\mathbf{x})\, \mathrm{d}\Gamma_{c3} \tag{3}$$

Let the given external actions $\bar{\mathbf{p}}$, $\bar{\mathbf{u}}$ act on two complementary disjoints of the boundary, say Γ_p and Γ_u respectively, and consider only the fictitious boundary. Betti's reciprocity identify holds for any source distribution $\mathbf{D}^*$, $\mathbf{F}^*$, $\mathbf{U}^*$, $\mathbf{V}^*$ and $\mathbf{W}^*$. If there is no traction acting on the fictitious crack surface, i.e. $\mathbf{F}^*$ is equal to zero, Let $\mathbf{D}^* = 0$ on Γ^*_u, $\mathbf{U}^* = 0$ on Γ^*_{c1}, $\mathbf{V}^* = 0$ on Γ^*_{c2}, and $\mathbf{W}^* = 0$ on Γ^*_{c3}, then Eq. (1) reduces further to:

$$\int_{\Gamma^*_u} [\mathbf{F}^*(\boldsymbol{\xi})]^{\mathrm{T}} \mathbf{D}(\boldsymbol{\xi})\, \mathrm{d}\Gamma_\xi = 0 \tag{4}$$

Since $[\mathbf{F}^*(\boldsymbol{\xi})]^{\mathrm{T}}$ can not be equal to zero, therefore $\mathbf{D}(\boldsymbol{\xi})$ must be equal to zero along the fictitious boundary. Consider the unconstrained Γ_p and the constrained Γ_u boundary portions respectively along the actual boundary. Setting Eq. (2) equal to zero, then following expression can be obtained:

$$\int_{\Gamma_u} \mathbf{G}_{uu}(\boldsymbol{\xi}, \mathbf{x})\mathbf{p}(\mathbf{x})\, \mathrm{d}\Gamma_x - \int_{\Gamma_u} \mathbf{G}_{up}(\boldsymbol{\xi}, \mathbf{x}; \mathbf{v}, /)\bar{\mathbf{u}}(\mathbf{x})\, \mathrm{d}\Gamma_x + \int_{\Gamma_p} \mathbf{G}_{uu}(\boldsymbol{\xi}, \mathbf{x})\bar{\mathbf{p}}(\mathbf{x})\, \mathrm{d}\Gamma_x - \int_{\Gamma_p} \mathbf{G}_{up}(\boldsymbol{\xi}, \mathbf{x}; \mathbf{v}, /)\mathbf{u}(\mathbf{x})\, \mathrm{d}\Gamma_x + \int_{\Gamma_{c1}} \mathbf{G}_{up}(\boldsymbol{\xi}, \mathbf{x}; \mathbf{v}, /)\mathbf{k}(\mathbf{x})\, \mathrm{d}\Gamma_{c1} + \int_{\Gamma_{c2}} \mathbf{G}_{up}(\boldsymbol{\xi}, \mathbf{x}; \mathbf{v}, /)\mathbf{l}(\mathbf{x})\, \mathrm{d}\Gamma_{c2} + \int_{\Gamma_{c3}} \mathbf{G}_{up}(\boldsymbol{\xi}, \mathbf{x}; \mathbf{v}, /)\mathbf{m}(\mathbf{x})\, \mathrm{d}\Gamma_{c3} = 0 \tag{5}$$

Similarly, other equations can be derived from Eq. (1). Then, the final matrix can be written as

$$\begin{bmatrix} \widetilde{\mathbf{G}}_{uu}^{uu} & -\widetilde{\mathbf{G}}_{up}^{up} & \widetilde{\mathbf{G}}_{up}^{uc1} & \widetilde{\mathbf{G}}_{up}^{uc2} & \widetilde{\mathbf{G}}_{up}^{uc3} \\ -\widetilde{\mathbf{G}}_{pu}^{pu} & \widetilde{\mathbf{G}}_{pp}^{pp} & -\widetilde{\mathbf{G}}_{pp}^{pc1} & -\widetilde{\mathbf{G}}_{pp}^{pc2} & -\widetilde{\mathbf{G}}_{pp}^{pc3} \\ \widetilde{\mathbf{G}}_{pu}^{c1u} & -\widetilde{\mathbf{G}}_{pp}^{c1p} & \widetilde{\mathbf{G}}_{pp}^{c1c1} & \widetilde{\mathbf{G}}_{pp}^{c1c2} & \widetilde{\mathbf{G}}_{pp}^{c1c3} \\ \widetilde{\mathbf{G}}_{pu}^{c2u} & -\widetilde{\mathbf{G}}_{pp}^{c2p} & \widetilde{\mathbf{G}}_{pp}^{c2c1} & \widetilde{\mathbf{G}}_{pp}^{c2c2} & \widetilde{\mathbf{G}}_{pp}^{c2c3} \\ \widetilde{\mathbf{G}}_{pu}^{c3u} & -\widetilde{\mathbf{G}}_{pp}^{c3p} & \widetilde{\mathbf{G}}_{pp}^{c3c1} & \widetilde{\mathbf{G}}_{pp}^{c3c2} & \widetilde{\mathbf{G}}_{pp}^{c3c3} \end{bmatrix} \begin{Bmatrix} \mathbf{U}^p \\ \mathbf{P}^u \\ \mathbf{K}^u \\ \mathbf{L}^u \\ \mathbf{M}^u \end{Bmatrix} = \begin{Bmatrix} \widetilde{\mathbf{G}}_{up}^{uu}\mathbf{U}^u - \widetilde{\mathbf{G}}_{uu}^{up}\mathbf{P}^p \\ \widetilde{\mathbf{G}}_{pp}^{pu}\mathbf{U}^u - \widetilde{\mathbf{G}}_{pu}^{pp}\mathbf{P}^p \\ \widetilde{\mathbf{G}}_{pp}^{c1u}\mathbf{U}^u - \widetilde{\mathbf{G}}_{pu}^{c1p}\mathbf{P}^p \\ \widetilde{\mathbf{G}}_{pp}^{c2u}\mathbf{U}^u - \widetilde{\mathbf{G}}_{pu}^{c2p}\mathbf{P}^p \\ \widetilde{\mathbf{G}}_{pp}^{c3u}\mathbf{U}^u - \widetilde{\mathbf{G}}_{pu}^{c3p}\mathbf{P}^p \end{Bmatrix} \tag{6}$$

where

$$\widetilde{\mathbf{G}}_{hk} = \int\int \left[\boldsymbol{\Psi}_{h'}^*(\boldsymbol{\xi})\right]^{\mathrm{T}} \mathbf{G}_{hk}(\boldsymbol{\xi}, \mathbf{x}) \boldsymbol{\Psi}_{k'}(\mathbf{x})\, \mathrm{d}\Gamma_x\, \mathrm{d}\Gamma_\xi \quad h,k = u,p; \quad h',k' = p,u \tag{7}$$

The partition of the matrices $\widetilde{\mathbf{G}}_{hk}$ is subordinate to the one defined by Eq. (7). The first superscript in the coefficient matrix of Eq. (6) indicates the location on Γ of the auxiliary sources; the second superscript denotes the location on Γ of the real quantity concerned. The proof of symmetry of $\widetilde{\mathbf{G}}_{hk}$ can be found in paper Sirtori et al. (1992). The system matrix of Eq. (6) is completely symmetric.

The numerical method relies on a double integration to establish the system coefficient matrix. Sirtori et al. (1992) had proposed a complex function method to get the analytical solutions of the double integrals using constant traction and linear displacement interpolation. For high order formulae $\overline{\boldsymbol{\Psi}}$, the second interpolation functions can be written for the boundary as:

$$\begin{aligned} \boldsymbol{\varphi}_u(\mathbf{x}) &= \boldsymbol{\Phi}_u(\mathbf{x})\overline{\boldsymbol{\Psi}}_u \\ \boldsymbol{\varphi}_p(\mathbf{x}) &= \boldsymbol{\Phi}_p(\mathbf{x})\overline{\boldsymbol{\Psi}}_p \end{aligned} \tag{8}$$

Based on the second stage interpolation functions, Eq. (7) can be rewritten as:

$$\widetilde{\mathbf{G}}_{ij} = \int\int \boldsymbol{\varphi}_{i'}^{\mathrm{T}}(\mathbf{x}) \mathbf{G}_{ij}(\mathbf{x}, \boldsymbol{\xi}) \boldsymbol{\varphi}_{j'}(\boldsymbol{\xi})\, \mathrm{d}\mathbf{x}\, \mathrm{d}\boldsymbol{\xi}, \quad i,j = u,p \quad i',j' = p,u \tag{9}$$

After substituting Eq. (8) into Eq. (9), then Eq. (9) becomes:

$$\widetilde{\mathbf{G}}_{ij} = \overline{\boldsymbol{\Psi}}_{i'}^{\mathrm{T}} \int\int \boldsymbol{\Phi}_{i'}^{\mathrm{T}}(\mathbf{x}) \mathbf{G}_{ij}(\mathbf{x}, \boldsymbol{\xi}) \boldsymbol{\Phi}_{j'}(\boldsymbol{\xi})\, \mathrm{d}\mathbf{x}\, \mathrm{d}\boldsymbol{\xi} \overline{\boldsymbol{\Psi}}_{j'}, \quad i,j = u,p \quad i',j' = p,u \tag{10}$$

The double integration of Eq. (10) can be solved analytically using the complex conjugate coordinates described in Sirtori et al. (1992). The integration order follows the sub-element and elements numberings. After the integration of each pair of elements has been performed, the coefficient is added into the main matrix. The coefficient in Eq. (10) can be expressed as:

$$\widetilde{\mathrm{G}}_{ijrs}^{ef} = \sum_{m}^{L} \sum_{n}^{L} \overline{\Psi}_{i'mr}^{e} \int\int \Phi_{i'mr}^{e}(\mathbf{x}) \mathrm{G}_{ijrs}^{ef}(\mathbf{x}, \boldsymbol{\xi}) \Phi_{j'ns}^{f}(\boldsymbol{\xi})\, \mathrm{d}\mathbf{x}\, \mathrm{d}\boldsymbol{\xi} \overline{\Psi}_{j'ns}^{f} \tag{11}$$

where r and s are the node numbers. e and f are the components of point variables. i and j denote the characteristic of variable as displacement or traction, m and n are the number of sub-elements. The two summations refer to the sub-elements contribution.

3. Stress intensity factor calculation and fatigue life estimation

Fracture mechanics has proved to be a useful tool in the fracture safe design and assessment of engineering structures and components. It can be used to predict the fatigue life of a welded joint. The rate of fatigue crack propagation of a welded joint containing a pre-existing crack can be evaluated from the range of stress intensity factor ΔK.

For the quarter-point elements used on the crack tip, the stress intensity factors K_I and K_{II} can be evaluated using following equations (Aliabadi and Rooke, 1991)

$$K_I = \frac{G}{\kappa + 1}\sqrt{\frac{2\pi}{l_t}}[4(v_B - v_D) - (v_E - v_C)] \tag{12}$$

$$K_{II} = \frac{G}{\kappa + 1}\sqrt{\frac{2\pi}{l_t}}[4(u_B - u_D) - (u_E - u_C)] \tag{13}$$

where u_C, u_E, u_B, u_D and v_C, v_E, v_B, v_D are the shearing and opening displacements at the opposite end-notes C and E, and at the opposite 1/4 point nodes B and D in the quarter-point element, l_t is the length of the side of the element internally adjacent to the front, $G = E/2(1 + v)$ is the shear modulus. $\kappa = (3 - 4v)$ for plane strain and $\kappa = (3 - v)/(1 + v)$ for plane stress.

The fatigue crack propagation of most welded joints can be estimated by

$$\frac{da}{dN} = C\Delta K^3 \tag{14}$$

where da/dN is the crack propagation rate in mm per cycle; and ΔK is the range of the stress intensity factor at the crack tip. The constant C depends on the material and testing conditions and it is taken to be 1.832×10^{-13} (Gurney, 1979).

Rearranging the above equation and integrating so that the variables a and N are separated produces

$$N = \int_0^N dN = \int_{a_1}^{a_2} \frac{1}{C}\Delta K^{-3}\, da \tag{15}$$

where a_1 and a_2 are the initial and final crack lengths for the particular geometry. The lack of penetration at the root of the weld has been observed to terminate at a sharp crack-like tip. The lack of penetration, therefore, can be treated as the initial crack in evaluating Eq. (15).

The value of ΔK in Eq. (15) for a crack at the weld root of a cruciform joint has been first numerically determined using a finite element solution by Frank (1971). The expression of ΔK is given in BS7608 (1993) in the form of M_k

$$\Delta K = M_k \Delta\sigma \left\{ \pi a \sec\left(\frac{\pi a}{2w + T}\right)\right\}^{0.5} \tag{16}$$

where $\Delta\sigma$ is the stress range in the loaded plate, and M_k is the magnification factor which is defined as the ratio of the stress intensity factor with stress concentration to the stress intensity factor for the same crack in plate without stress concentration. The term $\sigma\left\{\pi a \sec\left(\frac{\pi a}{2w+T}\right)\right\}^{0.5}$ is the stress intensity factor of an embedded crack of length $2a$ in a finite plate of thickness $2w + T$.

From Eq. (15), the fatigue life N can be estimated using a suitable numerical integration technique. The initial crack length a_1 will depend on the degree of weld penetration, and the final crack length a_2 on the strength and fracture toughness of the weld metal and the maximum stress applied. It was described by

Frank and Fisher (1979) that the actual mode of failure is not by continued vertical crack extension but by a shearing through the weld after the crack has extended a considerable distance into the weld. Furthermore, it was mentioned that the difference in the estimated fatigue life using measured values of a_2, and setting a_2 equal to $w + T/2$ is negligible.

4. Numerical results

The load-carrying fillet joints containing an edge crack and two embedded cracks as depicted in Fig. 3, is analyzed using the SGBEM codes developed based on the theory described in Section 2. Fig. 3 illustrates the numerical model used for the analysis. For this case, values of $\lambda = 1.0$ and $\gamma = 1.0$ resulting in $2a = 12.5$ mm and $w = 12.5$ mm, are used in the analysis. There are a total of 65 boundary elements used along the exterior boundary, and each of the embedded crack is discretized using six elements, while the edge crack is divided into seven elements. The quarter-point elements are used at all the cracks tip. Its length is always maintained to 5% of the crack length. It is best that the ratio of the two adjacent elements lengths is kept in the range of 1–2. The left extremity nodes are restrained against displacement in the x-direction, and also the mid-point node is restrained against displacement in the y-direction.

When the values of λ and γ are varied, the main plate thickness T and the 0.15 mm edge crack are unchanged. The number of boundary elements along the edge crack is kept the same and also along the embedded cracks. In this way, only the weld leg length w and the crack length $2a$ are constantly varied to determine the effect of these two parameters on the stress intensity factors at all the cracks tip. The analysis results by varying $\gamma = 0.2$, 0.4, 0.6, 0.8, 1.0 ($2a = 2.5$ mm, 5.0 mm, 7.5 mm, 10.0 mm, 12.5 mm) and $\lambda = 0.2$, 0.4, 0.6, 0.8, 1.0, 1.2, 1.4, 1.6, 1.8 ($w = 2.5$ mm, 5.0 mm, 7.5 mm, 10.0 mm, 12.5 mm, 15.0 mm, 17.5 mm, 20.0 mm, 22.5 mm), are obtained in this paper.

4.1. Stress intensity factor

Using the symmetric Galerkin boundary element method, the stress intensity factor (SIF) at the weld toe and weld root can be calculated directly using two-point crack-open-displacement formulae. Fig. 4 summarizes the values of SIF at weld root with values of $\gamma = 2a/T$ ranging from 0.2 to 1.0, and $\lambda = w/T$ from 0.2 to 1.8. The results are compared with those obtained by Lie and Bian (1997) using dual boundary element method (DBEM). The results are consistent using different methods. For the same weld size λ, the SIF in-

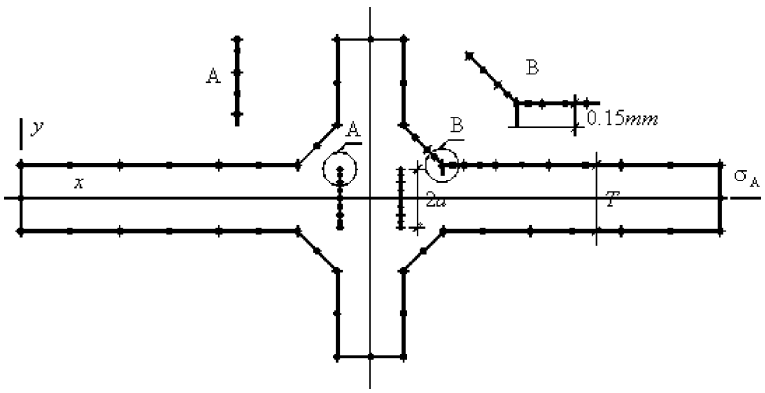

Fig. 3. Discretization modeling for symmetric Galerkin boundary element method.

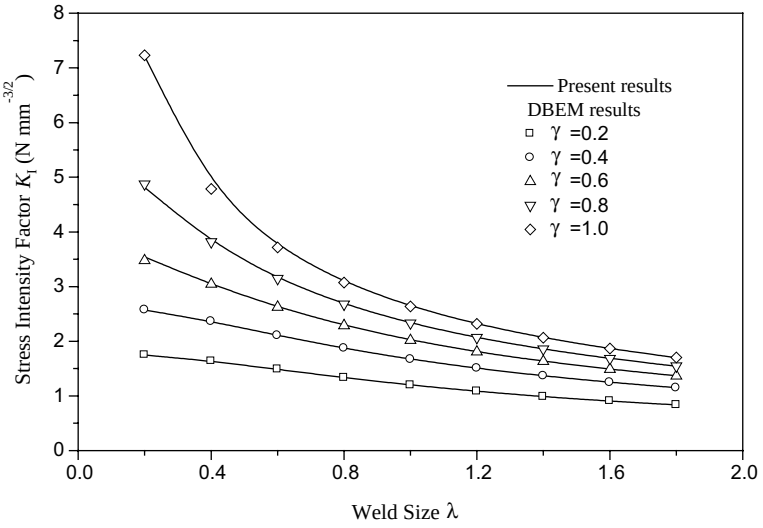

Fig. 4. Effect of weld size on SIF K_I (N mm$^{-3/2}$) at weld root for $T = 12.5$ mm.

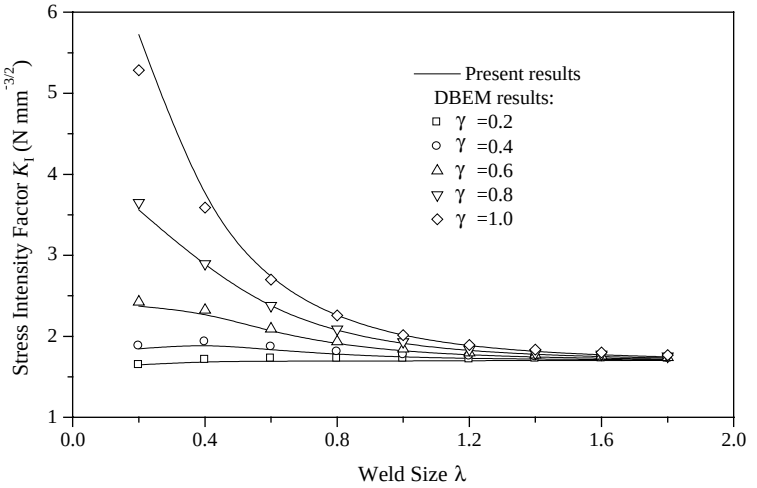

Fig. 5. Effect of weld size on SIF K_I (N mm$^{-3/2}$) at weld toe for $T = 12.5$ mm.

creases with the increase of crack length $\gamma = 2a/T$. They all decrease with the increase of weld size. Fig. 5 summarizes the values of SIF at weld toe. The SIF at toe increases with the increase of the embedded crack length. But with the weld size increases, the effect of the embedded crack decreases. These results can also be expressed clearly by plotting the SIFs against the value of $\lambda = w/T$ for a fixed value of embedded crack length $\gamma = 2a/T$. From a typical graph such as that of Fig. 6, it can be seen that when λ is less than 0.912, the SIF at the weld root is always higher than at the weld toe. By increasing the value of λ, the corresponding SIF at the weld root decreases at a faster rate than at the weld toe until both the SIFs are equal at a certain value of λ. This certain value of λ is the critical value for the crack to propagate from the weld root. If λ is greater than 0.912, then the SIF at the weld toe will be more dominant than at the weld root and

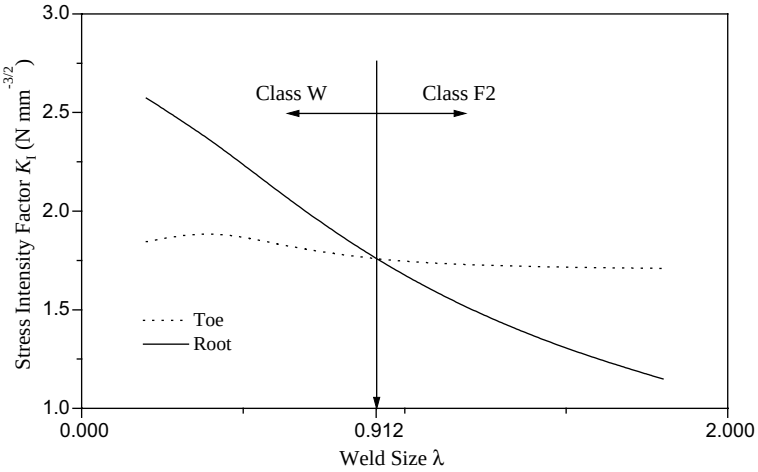

Fig. 6. Effect of weld size on SIF at weld root and weld toe for crack length $2a = 5$ mm.

the crack will likely to propagate from the weld toe. For each value of γ, there exists a value of λ for which both the SIFs at the weld toe and weld root are equal.

By plotting $\gamma = 2a/T$ against $\lambda = w/T$ as illustrated in Fig. 7, the classification of class F2 and class W can be established. If the value of λ and its corresponding value of γ lies on the line, it means that the values of SIF at the weld root and weld toe are equal; if it is below the line, the welded joint is classified as class F2; if it is above the line, it will then be classified as class W. The curve of the critical value can be expressed as

$$\gamma = 0.1689 + 0.2762\lambda^2 \tag{17}$$

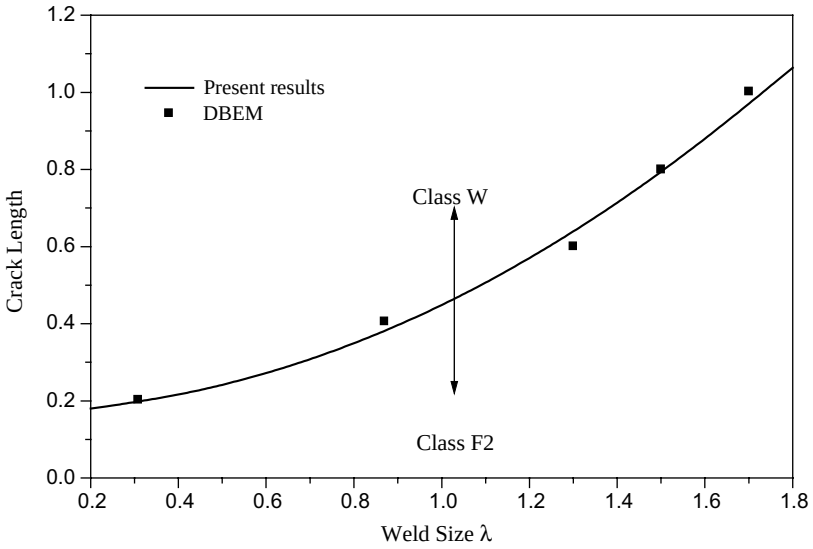

Fig. 7. Critical value of weld root crack length $\gamma = 2a/T$ and weld size $\lambda = w/T$ for class F2 and class W ($T = 12.5$ mm).

From the above results, it can be seen that for the load-carrying welded fillet, both the degree of weld penetration and weld size will affect the crack propagation pattern. Therefore, before the fatigue life and fatigue crack propagation path can be calculated, it is necessary to check the classification of this type of welded joint.

4.2. Magnification factor M_k

The magnification factor M_k can be calculated directly using the results of SIF obtained from SGBEM and the handbook Murakami (1987). The results of the corresponding M_k are plotted against the crack length ratio α in a log–log scale as shown in Fig. 8. The results obtained by Lie and Bian (1997) and BS7608 (1993) are also shown in the Fig. 8. From the figure, the three results are consistent with varying of weld size and crack length. Unlike the stress intensity factor, for a fixed value of weld size w, the magnification factor M_k at weld root does not always increase while the internal crack length $\alpha = 2a/(2w + T)$ is increased. The graph shows that when weld size w is less than 10 mm, M_k increases by increasing the internal crack length $2a$. At smaller weld size w, the increase in M_k is steeper. When the weld size is more than 10 mm, M_k is observed to decrease gradually by increasing the internal crack length $2a$. Such a tendency means that increasing the weld size w can decrease the stress concentration at the weld root effectively as this is reflected by the value of M_k at the crack tip.

The M_k is very sensitive to changes made to the SIF. This is confirmed from the SGBEM analysis that a small change in SIF will have a significant influence in M_k. The difference from the three methods is more obvious for smaller value of $\alpha = 2a/(2w + T)$. The smaller the value of $\alpha = 2a/(2w + T)$ is, the more sensitive M_k is. Thus, it is very important to obtain a high degree of accuracy for the stress intensity factors at the weld root.

4.3. Fatigue life estimation

The fatigue life for Class W joints for the fixed value of $\lambda = 0.2$ and 1.2 can be estimated using Eq. (15). The initial crack length a_1 is determined from Eq. (17) to ensure that the crack will propagate from the weld

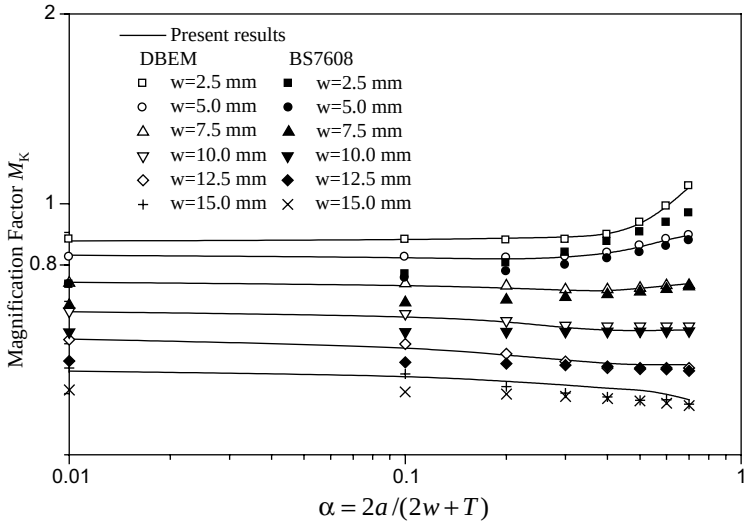

Fig. 8. Effect of weld size on the magnification factor at weld root for $T = 12.5$ mm.

root. The final crack length a_2 are equal to $w + T/2$. The magnification factors for $\lambda = 0.2$ and 1.2 can be expressed as

$$M_k = 0.8752 + 0.7369 \times \left(\frac{2a}{2w+T}\right)^{3.8086} \quad \lambda = 0.2$$
$$M_k = 0.4421 + 0.1011 \times e^{-\frac{2a}{2w+T}} \quad \lambda = 1.2 \tag{18}$$

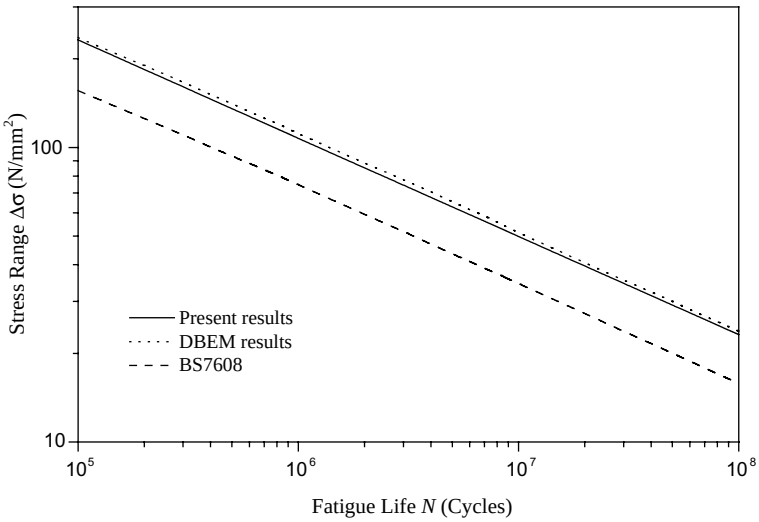

Fig. 9. Fatigue life N of class W for $\lambda = 0.2$ ($T = 12.5$ mm).

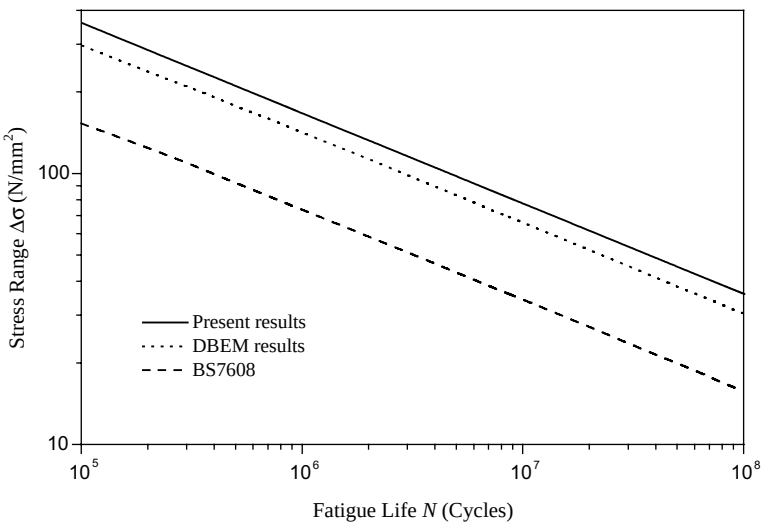

Fig. 10. Fatigue life N of class W for $\lambda = 1.2$ ($T = 12.5$ mm).

Substitute the Eqs. (16) and (18) into Eq. (15). The fatigue life can be estimated and the integral results can be expressed as

$$\begin{aligned} N &= 1.2423 \times 10^{12} \Delta\sigma^{-3} \quad \lambda = 0.2 \\ N &= 4.6597 \times 10^{12} \Delta\sigma^{-3} \quad \lambda = 1.2 \end{aligned} \tag{19}$$

The results are plotted in log-log scale in Figs. 9 and 10. From the curves shown in these figures, the results obtained from SGBEM are very close to the results obtained from DBEM. They are consistently higher than those obtained from BS7608 (1993).

5. Conclusions

The symmetric boundary element method for multiple cracks problem is derived using Betti's reciprocal theorem. High order element is proposed to solve the double integrals. The analysis can be performed effectively for the analyzing the load-carrying fillet welded joints containing any number of surfaces and embedded cracks. The stress intensity factors are calculated for weld root and weld toe. It is shown from Fig. 6 that there is a certain ratio of $\lambda = w/T$ at which the stress intensity factors at the weld toe and root are equal for a fixed value of $\gamma = 2a/T$. Fig. 7 summarizes the analysis for $\gamma = 2a/T$ ranging from 0.2 to 1.2 and $\lambda = w/T$ from 0.2 to 1.8. The results are then used to establish the classification of Class F2 or Class W load-carrying fillet welded joints. Formulation for the critical value is obtained for the engineering design. Using the values of the stress intensity factor, the magnification factor M_k can be deduced. Finally, the theoretical fatigue life of such joints is calculated. The fatigue life for load-carrying weld joints are estimated and they are consistent with those obtained by DBEM and higher than code BS7608 (1993). This can provide a good method for engineering design under fatigue loading conditions.

References

Aliabadi, M.H., Rooke, D.P., 1991. Numerical Fracture Mechanics. Computational Mechanics Publications, Southampton.

BS7608, 1993. Code of practice for fatigue design and assessment of steel structures. British Standard 7608. British Standard Institution, London, England.

Frank, K.H., 1971. The fatigue strength of fillet welded connections. Ph.D. Thesis. Lehigh University.

Frank, K.H., Fisher, J.W., 1979. Fatigue strength of fillet welded cruciform joints. J. Struct. Div. ASCE 105 (9), 1727–1740.

Gurney, T.R., 1979. Theoretical analysis of the influence of attachment size on the fatigue strength of transverse non-load-carrying fillet welds. Research Report 91/1979, The Welding Institute, Cambridge.

Lie, S.T., Bian, C., 1997. Load-carrying fillet welds using dual boundary element method. J. Struct. Eng. 123 (12), 1603–1613.

Lie, S.T., Xu, K., Cen, Z., 1999. Multiple crack analysis using symmetric Galerkin boundary element method. In: 4th Asia-Pacific Conference on Computational Mechanics, Singapore. pp. 353–358.

Murakami, Y., 1987. Stress Intensity Factors Handbook. Pergamon Press, Elmsford, New York, USA.

Sirtori, S., Maier, G., Novati, G., Miccoli, S., 1992. A Galerkin symmetric boundary element method in elasticity: formulation and implementation. Int. J. Numer. Meth. Eng. 35 (2), 255–282.